Supporting Information (SI APPENDIX).

SI METHODS

Generation of hiPSCs. 60,000 fibroblasts were electroporated with 1 µg each of pCXLE-hOCT4-shP53, pCXLE-hSK and pCXLE-hUL plasmids (plasmids gifts from Prof. S. Yamanaka; Addgene plasmids #27077, 27078, 27080) using the nucleofection kit for primary fibroblasts (Lonza) and nucleofected using the Nucleofector 2b Device (Lonza, Program T-016). Cells were cultivated in fibroblast medium for 6 days and then 1 x 10^5 cells trypsinized cells were plated onto a 10 cm dish with irradiated mouse embryonic fibroblast (MEF) feeders. Medium was changed to hiPSC basal medium (DMEM/F12 with 20% Knockout serum replacement or KSR, 1% MEM-NEAA, 1% glutamax and 100 ng/mL FGF2; Thermo Fisher Scientific) the following day. hiPSC colonies started appearing around day 17-30 from transfection and were manually dissected and expanded for further characterisation.

Differentiation of hiPSCs to RPE cells. hiPSC colonies were lifted and then cultured in suspension in either hiPSC basal medium depleted of FGF or mTESR to generate embryoid bodies (EBs). On day 6 post EB generation, EBs were plated to laminin coated plate in neural induction medium (NIM, DMEM/F12 with 1% MEM-NEAA, 1% N-2 Supplement; Thermo Fisher Scientific) and 2 µg/mL heparin (Thermo Fisher Scientific). At day 14, the cell growth medium was switched from NIM to retinal differentiation medium (RDM, 70% DMEM / 30% F-12 with B-27 supplement; Thermo Fisher Scientific). At ~day 20, optic vesicle-like structures were removed as previously described (1, 2) and the remaining cells were allowed to grow as adherent cultures. To

passage hiPSC-RPE cells after dissection, cells were dissociated with 0.05% Trypsin-EDTA and plated onto 24 well plates and/or transwells coated with laminin for 4-24h. hiPSC-RPE cells were thereafter cultured in RDM media containing 2% fetal bovine serum (FBS) until the cells had formed a confluent monolayer. After reaching confluence, FBS was removed from the cell culture media and cells were maintained exclusively in RDM. Similarly, for passaging RPE cells, mature monolayers of RPE cells were trypsinized and re-plated using the protocol described above.

Extracellular matrix (ECM) isolation. hiPSC-RPE were removed by incubation with 10 mM EDTA in 1x phosphate buffer saline (PBS) at 37 °C for up to 60 min in 20 min intervals (3). After, confirmation of removal of all hiPSC-RPE cells by light microscopy, the underlying ECM was incubated in ECM isolation buffer (1% SDS and 10% glycerol in Tris buffer pH 6.8) with protease inhibitor cocktail (Sigma-Aldrich, St Louis, MO, P2714) for 30 minutes at 37°C (4). Freshly isolated ECM extract from Ctrl and patient (SFD, DHRD, ADRD) samples were either immediately stored in -80°C or further analyzed by Western blotting.

Transepithelial resistance (TER) measurement. hiPSC-RPE were plated at a density of 50,000 cells/well onto 6.5 mm diameter transwell inserts with 0.4 µm pore size and cultured in RDM in accordance with our previously described protocol (5). TER was recorded using an EVOM2 volt-ohm meter (World Precision Instruments, Sarasota, FL), in accordance with the manufacturer's instructions. For each TER recording, an empty

transwell containing RDM (cell culture medium) alone served as the blank recording. Blank subtracted TER measurements were reported as resistance per area or $\Omega*cm^{-2}$.

Quantitative real-time RT-PCR analysis. RNA was isolated from hiPSC-RPE cells grown in transwells and/or 24 well plates using QiaShredder and the RNAeasy micro kit (Qiagen, Germantown, MD) in accordance with the manufacturer's instructions. The RNA thus isolated was subjected to DNase I treatment for 30 min to degrade any genomic DNA contamination. In every experiment, cDNA was synthesized using an equivalent amount of DNase I-treated Ctrl and patient (SFD, DHRD, ADRD) RNA using iScript reverse transcriptase kit (BioRad) in accordance with the manufacturer's protocol. Quantitative PCR was conducted using cDNA, SYBR Green (BioRad) and gene-specific primers on the CFX-Connect Real Time System cycler (BioRad). Primer pairs used for analysis of complement pathway genes and RPE markers (5), are listed in *Table S2* and *Table S3*. *GAPDH* served as a loading control and gene expression was calculated relative to *GAPDH*, then normalized to Ctrl samples in all experiments**.** Quantitative PCR data were analyzed using the Biorad CFX Manager 3.1 software and Microsoft Excel.

Western blot analysis. After transfer of protein sample on PVDF membranes, the PVDF membranes were incubated in blocking buffer, 5% dry milk in PBS and/or mammalian blocking buffer (Li-cor Biosciences, Lincoln, NE) for 1h at room temperature (RT), washed 4 times in PBS-tween (0.1%), followed by an overnight incubation in protein-specific primary antibody solution in blocking buffer at 4°C. This was followed by

4 washes in PBS and incubation in host-specific secondary antibody for 1h at RT. After 4 final washes in PBS, the PVDF membranes were visualized and analyzed using Li-cor Odyssey Model 9120 (Li-cor Biosciences), Azure C500 imaging system (Azure Biosystems, Dublin, CA) or exposure of chemiluminescence to film (GE Healthcare, Buckinghamshire, UK). Primary antibodies used for Western blot analysis included ACTN (1:750, Santa Cruz Biotechnology, Dallas, TX), BEST1 (1:500, Millipore, Billerica, MA), COL4 (1:1000, Abcam, Cambridge, MA), CRALBP (6), EZRIN (1:1000, Cell Signaling Technology, Danvers, MA), LAM (1:1000, Abcam), and RPE65 (1:500, Millipore). The secondary-antibodies used in this study included host-specific near-infrared (Li-cor, Azure Biosystems), HRP-conjugated (Jackson ImmunoResearch, West Grove, PA) and radiance plus HRP substrate (Azure Biosystems). Quantitative analyses of the Western blot data were carried out using the image acquisition software (Licor Odyssey 3.0 and/or Image Studio Lite version 5.2) and Microsoft Excel.

Processing of hiPSC-RPE samples for whole mount and sections. Mature monolayer of hiPSC-RPE grown in transwells and/or non-permeable plastic support were fixed in 4% paraformaldehyde for 30 min at 4°C. For whole mount analyses, no further processing was done and immunocytochemistry was performed as described below (see immunocytochemical analysis). For frozen sections, fixed hiPSC-RPE were washed 2X for 5 min each in PBS and then incubated in increasing sucrose density solutions; 10% for 1 hour, 20% for 1 hour and 30% over night. The next day hiPSC-RPE samples were submerged in tissue freezing media (Triangle Biomedical Sciences, Durham, NC), snap frozen, sectioned at 14 µm thickness on CRYOSTAR NX50

(Thermo Fisher Scientific) and either used directly for immunocytochemical analysis or stored at -20°C prior to further use. For paraffin sectioning, the entire well was fixed and dehydration process for paraffin embedding was started in the cell culture dish and thereafter fixed cells were lifted mechanically with gentle pressure and embedded in paraffin for sectioning and staining. Specifically, hiPSC-RPE monolayers were dehydrated by successive 30-minute incubation in 70, 95 and 100% ethanol and subsequently with an overnight incubation in 100% ethanol. The next day hiPSC-RPE samples were incubated in xylene, prior to paraffin embedding under vacuum. Paraffin blocks were sectioned at 14 µm thickness using HM 310 microtome (Microm, Walldorf, Germany). Furthermore, like frozen hiPSC-RPE sections, paraffin hiPSC-RPE sections were either used directly for immunocytochemical analysis or stored at 4°C prior to further use. Of note, to prepare for immunocytochemical analysis, slides containing paraffin hiPSC-RPE sections, were heated at 65°C for 15 minutes then cooled at room temperature prior to deparaffinization using two 10 minute washes in xylene. This was followed by re-hydration in successive washes 100%, 95%, and 70% ethanol, twice each for 3 minutes, before a final wash in ddH_2O for 3 min. Finally, antigen retrieval was carried out by incubating slides in 10 mM sodium citrate buffer pH 6.0 at ~95 °C for 30 minutes.

Immunocytochemical analysis. Fixed hiPSC-RPE whole mounts were blocked/permeabilized in 10% normal donkey serum (ImmunoReagents Inc., Raleigh, NC) and 0.1% triton-x-100 in 1X PBS (PBS-TX) for 1h. This was followed by an overnight incubation in protein-specific primary antibody solution in 0.5X blocking buffer

at 4°C. The next day, samples were washed 2 times in PBS-TX and incubated in host-specific secondary antibody for 1h at RT. This was again followed by 2 washes in PBS-TX and incubation in nuclear staining dyes, DAPI or Hoechst 33342 (Life Technologies) and/or neutral lipid stain (Nile red, Molecular Probes, Eugene, OR) for 15 min. in PBS. Slides/samples were subsequently mounted in Prolong gold (Life Technologies), coverslipped and imaged using either an inverted fluorescent microscope (DM IRB, Leica, Buffalo Grove, IL) or a confocal microscope (LSM 510 META, Zeiss, Thornwood, NY). Images were captured using Infinity Analyze (Luminera, Ottawa, Ontario) and Zen 2009 software (Zeiss) and analyzed further with Zen 2009 software and Image J software (NIH). Primary antibodies used for immunocytochemical analysis included**;** APOE (1:500, Millipore), BEST1 (1:50, Millipore), C3 (1:100, Abcam), C5b-9 (1:200, Agilent, Santa Clara, CA), COL4 (1:100, Abcam), CRYAA/CRYAB (1:100, Enzo, Farmingdale, NY), EFEMP1 (1:200, Abcam), EZRIN (1:1000, Cell Signaling Technology, Danvers, MA), NANOG (1:100, R&D systems, Minneapolis, MN) and Oct 3/4 (1:100, Santa Cruz Biotechnology), TIMP3 (1:100 Abcam or GeneTex, Irvine, CA) VTN (1:100, Millipore) and ZO-1 (1:100, Life Technologies). All secondary antibodies used in this study were Alexa-conjugated (Life Technologies) and used at a concentration of 1:500.

Availability of unique reagents to the study. Unique reagents can be obtained by contacting the corresponding author.

SI REFERENCES

1. Meyer JS*, et al.* (2011) Optic vesicle-like structures derived from humapluripotent stem cells facilitate a customized approach to retinal disease treatment. *Stem Cells* 29(8):1206-1218.

2. Meyer JS*, et al.* (2009) Modeling early retinal development with human embryonic and induced pluripotent stem cells. *Proc Natl Acad Sci U S A* 106(39):16698-16703.

3. Qi JH*, et al.* (2009) S156C mutation in tissue inhibitor of metalloproteinases-3 induces increased angiogenesis. *J Biol Chem* 284(30):19927-19936.

4. Weber BH*, et al.* (2002) A mouse model for Sorsby fundus dystrophy. *Invest Ophthalmol Vis Sci* 43(8):2732-2740.

5. Singh R*, et al.* (2013) iPS cell modeling of Best disease: insights into the pathophysiology of an inherited macular degeneration. *Hum Mol Genet* 22(3):593-607.

6. Saari JC, Nawrot M, Stenkamp RE, Teller DC, & Garwin GG (2009) Release of 11-cis-retinal from cellular retinaldehyde-binding protein by acidic lipids. *Mol Vis* 15:844-854.

SI TABLES

Table S1. Quantitative real-time PCR analyses of complement pathway genes in Ctrl vs. SFD, DHRD and ADRD hiPSC-RPE cultures. Data are presented as mean ± SEM. *=p<0.05, **=p<0.005.

Gene	CTRL	SFD	CTRL	DHRD	CTRL	ADRD
C1R	1 ± 0.24	1.96 ± 0.32 *	1 ± 0.13	1.26 ± 0.30	1 ± 0.23	3.40 ± 1.87
C1S	1 ± 0.21	2.08 ± 0.37 *	1 ± 0.18	1.34 ± 0.38	1 ± 0.37	1.19 ± 0.37
C3	1 ± 0.26	4.84 ± 1.20 **	1 ± 0.19	1.27 ± 0.46	1 ± 0.25	2.19 ± 0.96
C5	1 ± 0.10	0.90 ± 0.16	1 ± 0.18	1.73 ± 0.21 **	1 ± 0.24	2.49 ± 1.25
C7	1 ± 0.08	1.24 ± 0.27	1 ± 0.28	3.59 ± 2.57	1 ± 0.30	5.79 ± 2.43
CFB	1 ± 0.14	1.50 ± 0.42	1 ± 0.18	3.02 ± 1.21	1 ± 0.20	6.22 ± 3.14
CD59	1 ± 0.14	1.26 ± 0.48	1 ± 0.29	1.29 ± 0.41	1 ± 0.27	1.43 ± 0.70
CFHv1	1 ± 0.15	13.68 ± 9.46	1 ± 0.08	0.80 ± 0.20	1 ± 0.27	1.56 ± 0.88
CFHv2	1 ± 0.11	17.56 ± 11.22	1 ± 0.08	0.99 ± 0.34	1 ± 0.30	2.62 ± 0.84
DAF	1 ± 0.11	11.66 ± 7.98	1 ± 0.46	1.22 ± 0.18	1 ± 0.19	2.25 ± 0.65
MCP	1 ± 0.10	1.89 ± 0.39 *	1 ± 0.27	1.82 ± 0.43 *	1 ± 0.20	2.14 ± 0.70
SERPING1	1 ± 0.08	1.63 ± 0.32	1 ± 0.33	1.73 ± 0.64	1 ± 0.26	9.27 ± 5.07
VTN	1 ± 0.11	1.08 ± 0.29	1 ± 0.10	1.29 ± 0.53	1 ± 0.38	5.21 ± 1.90

Table S2: Primers pairs (5'-3') used for amplifying complement genes.

Gene	Forward Primer	Reverse Primer
C1R	AGAAAGACCGTGTGTGAAATTC	CAAAGTGGAAGAGGAAAGTGAC
C1S	ATCATAGAATTGTGCTGGTCATAC	GGTAAAGAGGAAACAAAGAATTAAGG
C3	GCTACATCATCGGGAAGGAC	CTGGCATTGTTTCTGGTTCTC
C5	TGGACTCCTGTTGTTGAAGTTC	AAAGCAAGTGCCACTAATTCTAAG
C7	AGGTAGATTAGTTTGAAGCATTGAC	CATTTAAGCCCTCTCATTTCTCC
CFB	CCCTATGCTGACCCCAATAC	GATTACACCAACTTGAATGAAACG
CD59	GACTTTGCCTCCTGACAGC	CCCTTACTCCAAGATAATCTAAACAG
CFHv1	AACAGATTGTCTCAGTTTACCTAGC	ACCCGCCTTATACACATCCTTC
CFHv2	CTTTACCCTCTGAACTTCTGATCG	TCTGGCTGGAATAATACACACATAAC
DAF	AACCCAATTCAGTCTCTTCTAAGC	CTCCCTTATCACCATCAACACC
MCP	GCACAGAGTTGAAGTTTATACCC	CACCATTATCTGCTTCTTAGTAATTG
SERPING1	GCAGCTTTCTCTAGTTCAAGTTC	TTGAAAGTCATGGTCTGTCAGG
VTN	GGATGGACTGGCTTGTGC	CCGTGTGCGAAGATTGACTC
GAPDH	AGCAAGAGCACAAGAGGAAGAG	GAGCACAGGGTACTTTATTGATGG

Table S3: Primers pairs (5'-3') used for amplifying RPE-signature genes.

Gene	Forward primer	Reverse primer
BEST1	ATTTATAGGCTGGCCCTCACGGAA	TGTTCTGCCGGAGTCATAAAGCCT
MERTK	AGCCTGAGAGCATGAATGTCACCA	TGTTGATCTGCACTCCCTTGGACA
MITF	TTCACGAGCGTCCTGTATGCAGAT	TTGCAAAGCAGGATCCATCAAGCC
PEDF	AGATCTCAGCTGCAAGATTGCCCA	ATGAATGAACTCGGAGGTGAGGCT
RPE65	GCCCTCCTGCACAAGTTTGACTTT	AGTTGGTCTCTGTGCAAGCGTAGT
OCCLUDIN	TCCTATAAATCCACGCCGGTTCCT	AGGTGTCTCAAAGTTACCACCGCT
CRALBP	TTCCGCATGGTACCTGAAGAGGAA	ACTGCAGCCGGAAATTCACATAGC

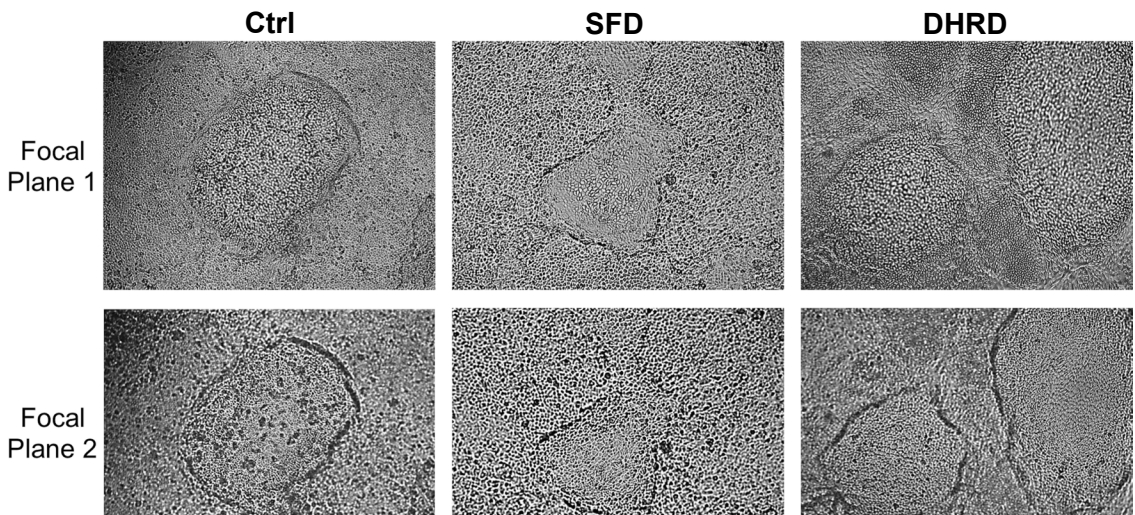

Fig. S1. Ctrl, SFD and DHRD hiPSC RPE form fluid domes when cultured on non-permeable plastic support. Light microscopy images displayed fluid-filled domes in aged (D90) Ctrl, SFD and DHRD hiPSC-RPE monolayers grown on non-porous supports confirming the polarized nature of hiPSC-RPE in culture. Of note, images in the top vs. bottom panels are taken on two different focal planes to demonstrate RPE monolayer both inside and outside of the fluid-filled domes in the Ctrl, SFD and DHRD hiPSC-RPE cultures (Scale bar = 100 µm).

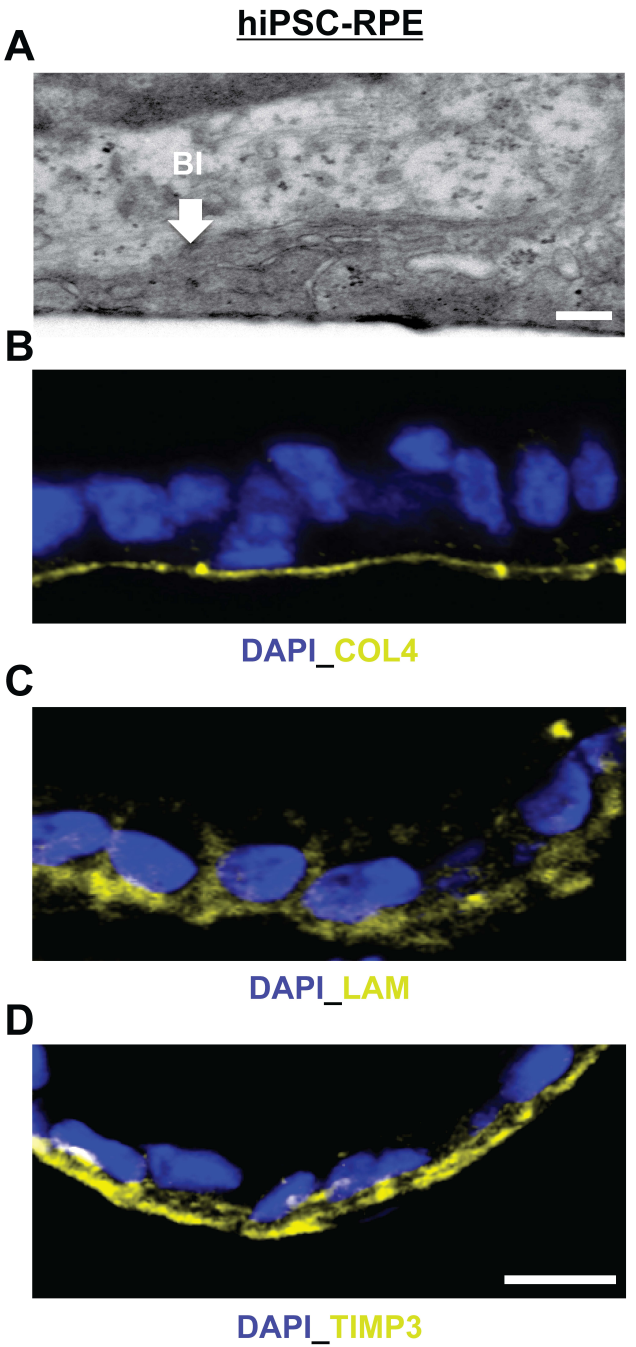

Fig. S2. hiPSC-RPE form a basement membrane with characteristics similar to human RPE cells in vivo. (A) Electron microscopy analyses showed basal infoldings (BI) in aged (D90) hiPSC-RPE culture grown on transwell inserts (Scale bar = 1 µm). (B-D) Immunocytochemical analyses of D90 hiPSC-RPE cross-sections on non-permeable plastic support demonstrated COL4, LAM and TIMP3 localization consistent with the presence of a basement membrane underneath hiPSC-RPE cells in culture (Scale bar = 12.5 µm).

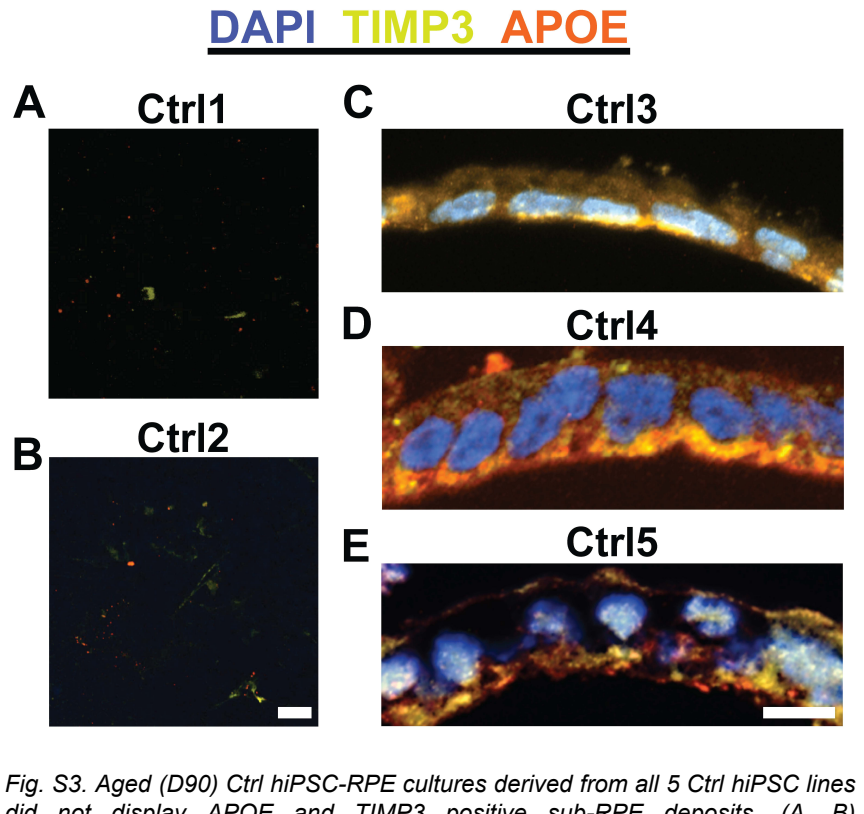

Fig. S3. Aged (D90) Ctrl hiPSC-RPE cultures derived from all 5 Ctrl hiPSC lines did not display APOE and TIMP3 positive sub-RPE deposits. (A, B) Immunostaining of transwell membranes after the removal of aged (D90) Ctrl1 and Ctrl2 hiPSC-RPE monolayers did not show sub-RPE deposits with co-localized APOE and TIMP3 (Scale bar = 25 μm). (C-E) Confocal images of Ctrl3, Ctrl4 and Ctrl5 hiPSC-RPE cross-sections from aged (D90) hiPSC-RPE cultures also did not display any sub-RPE deposits that demonstrated immunoreactivity for both APOE and TIMP3 (Scale bar = 12.5 μm).

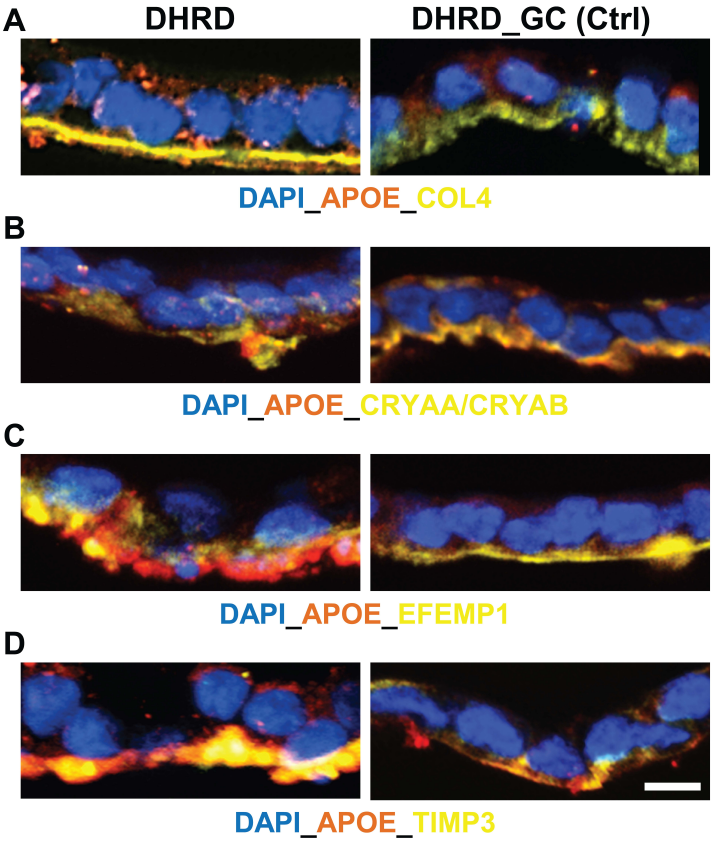

Fig. S4. Different composition of sub-RPE deposits underneath "aged" (D90) DHRD hiPSC-RPE compared to hiPSC-RPE derived from the isogenic gene-corrected DHRD hiPSC line (DHRD_GC, Ctrl4). Immunocytochemical analyses of cross-sections of aged (D90) DHRD-patient and gene-corrected isogenic Ctrl hiPSC-RPE (DHRD_GC) cultures revealed the expected localization of basement membrane proteins (A) COL4, (C) EFEMP1 and (D) TIMP3. Furthermore, confocal images showed presence of sub-RPE deposits containing (A) APOE underneath the basement membrane stained by COL4, (B) APOE-CRYAA/CRYAB, (C) APOE-EFEMP1 and (D) TIMP3-APOE only in patient-derived DHRD hiPSC-RPE (D90) (left panel) while DHRD_GC hiPSC-RPE was absent of similar deposits (right panels) (Scale bar = 12.5 µm).

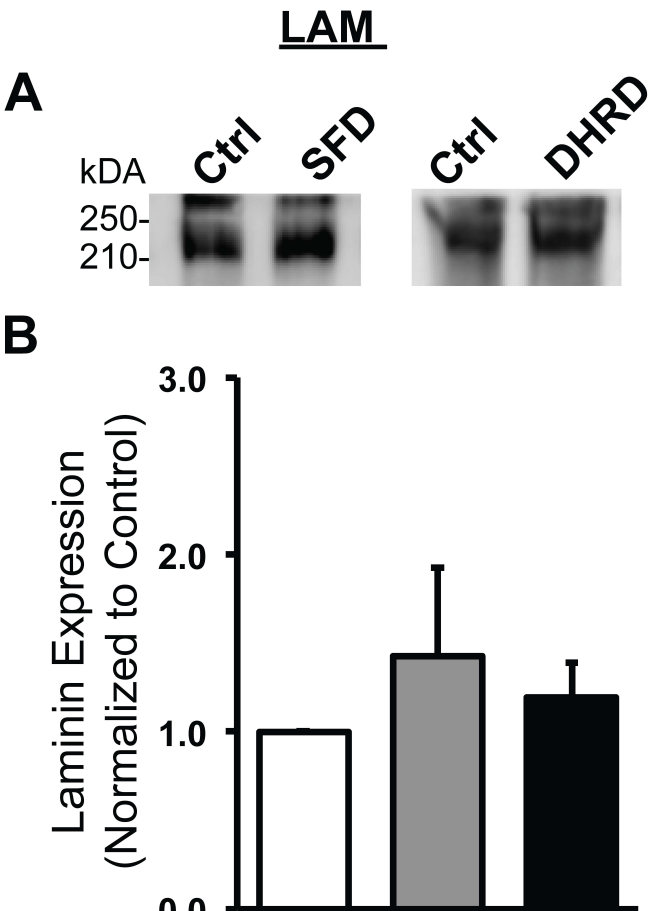

Fig. S5. Similar amount of LAM protein is present in the ECM underlying Ctrl vs. SFD and DHRD hiPSC-RPE cultures at D90. (A, B) Quantitative Western blot analyses demonstrated no difference in the abundance of LAM protein in the ECM underlying SFD and DHRD hiPSC-RPE cultures compared to Ctrl hiPSC-RPE cultures at D90. Of note, LAM bands at ~225 kDa (A) are consistent with β1 and β2 subunit of human LAM protein. Data are presented as mean + SEM.

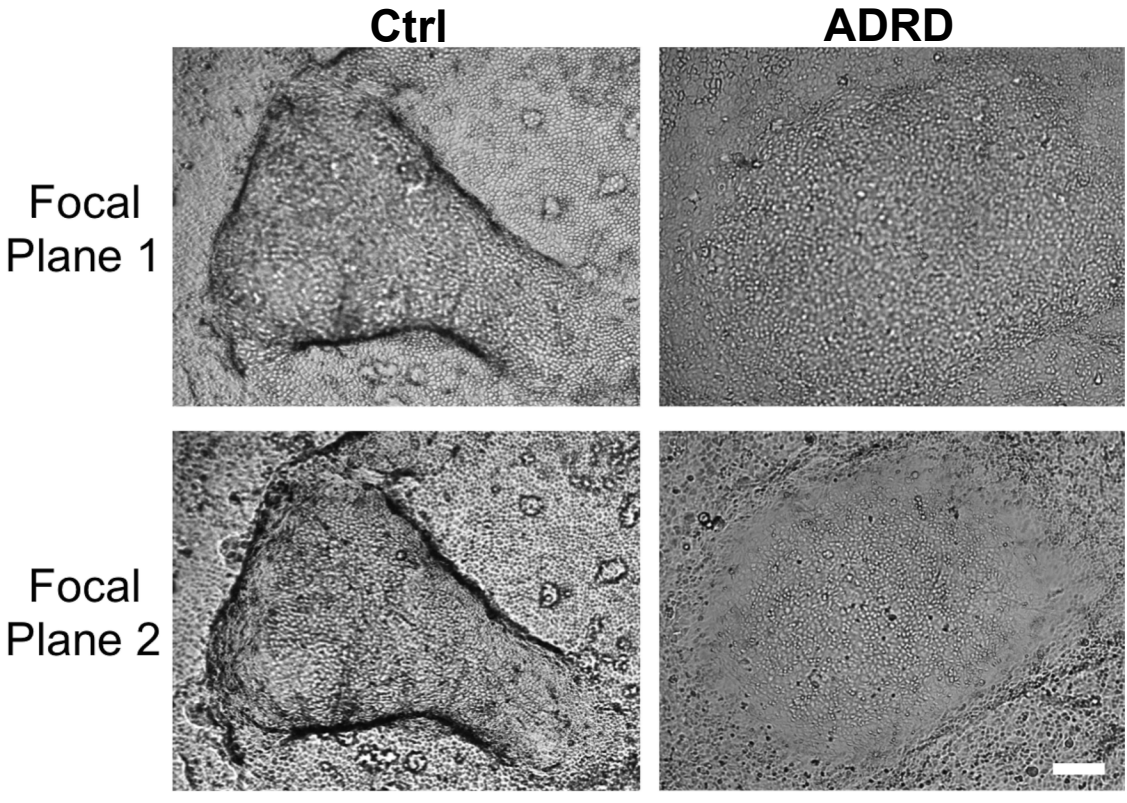

Fig. S6. ADRD hiPSC RPE form fluid domes similar to Ctrl hiPSC-RPE when cultured on non-permeable plastic support. Light microscopy images showed fluid-filled domes in aged (D90) cultures of both Ctrl and ADRD hiPSC-RPE grown on non-porous supports confirming their polarized nature in culture. Note: The top vs. bottom panel images are taken on two different focal planes to demonstrate the presence of RPE cells underneath the fluid-filled domes (Scale bar = 100 µm).

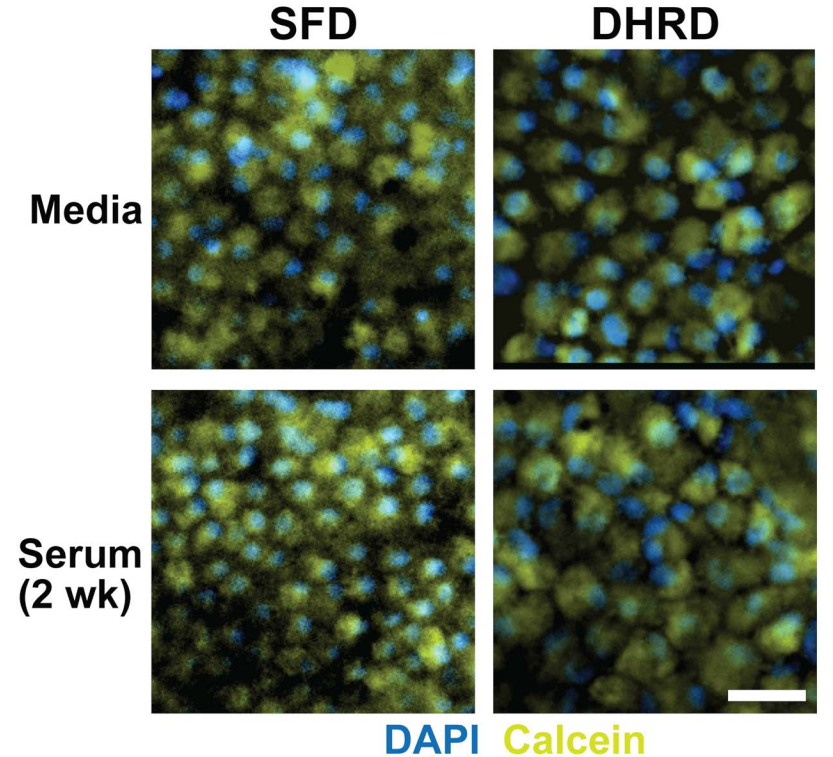

Fig. S7. Chronic serum supplementation (2 wk) does not affect the cellular viability of SFD and DHRD hiPSC-RPE in culture. Immunofluorescent imaging showed similar staining of Calcein-AM (live cells) in untreated (top panel) vs. serum-treated (bottom panel; 10%, 2 wk) SFD and DHRD hiPSC-RPE cultures (Scale bar = 50 μm).

Fig. S8

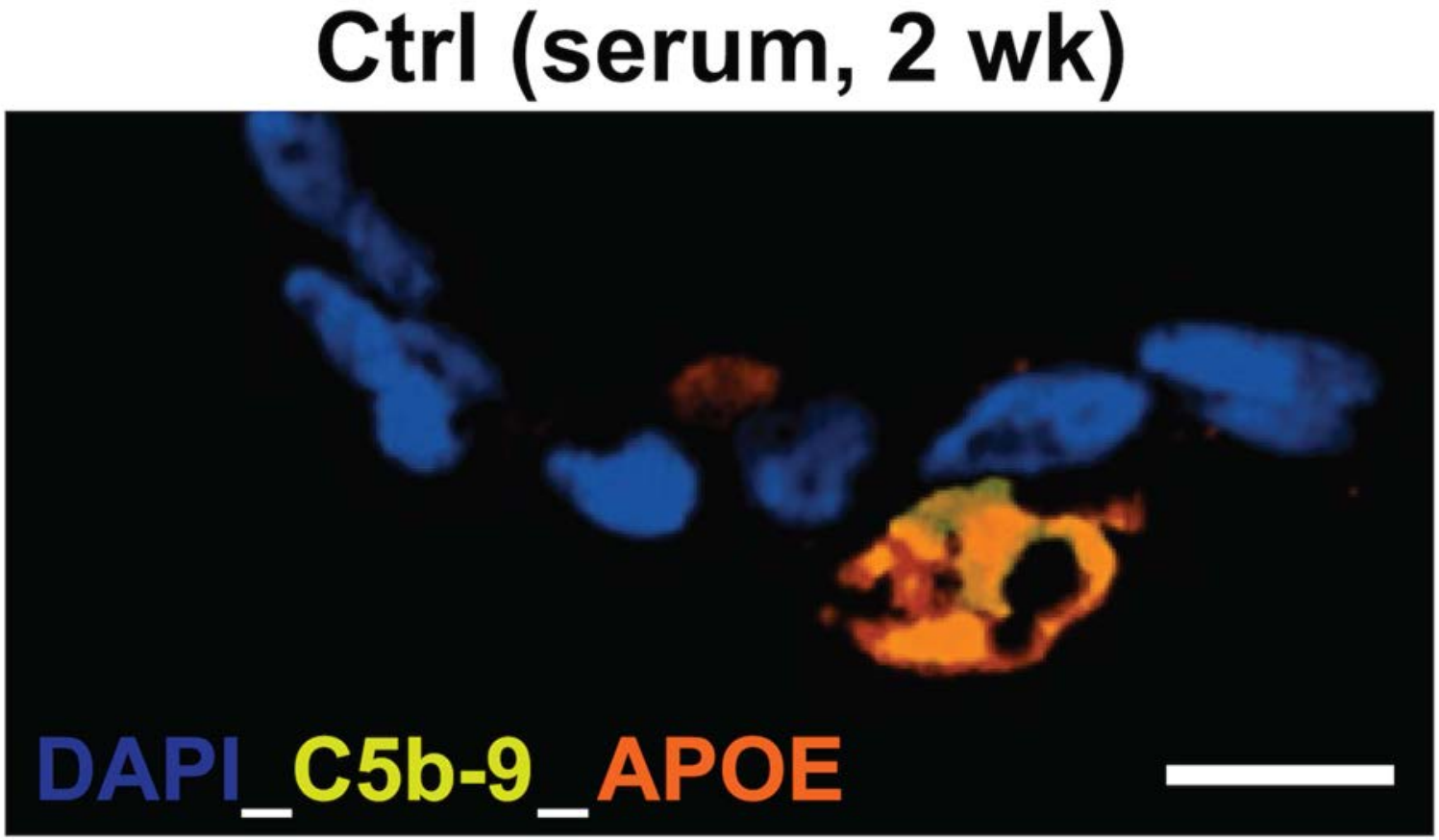

Fig. S8. Serum supplementation leads to formation of APOE and C5b-9 positive basal deposits in Ctrl hiPSC-RPE cultures. Confocal images demonstrated sub-RPE deposits with immunoreactivity for both complement proteins, C5b-9, and drusen marker (APOE) in Ctrl hiPSC-RPE after chronic serum supplementation (10%, 2 wk) (Scale bar = 25 μm).

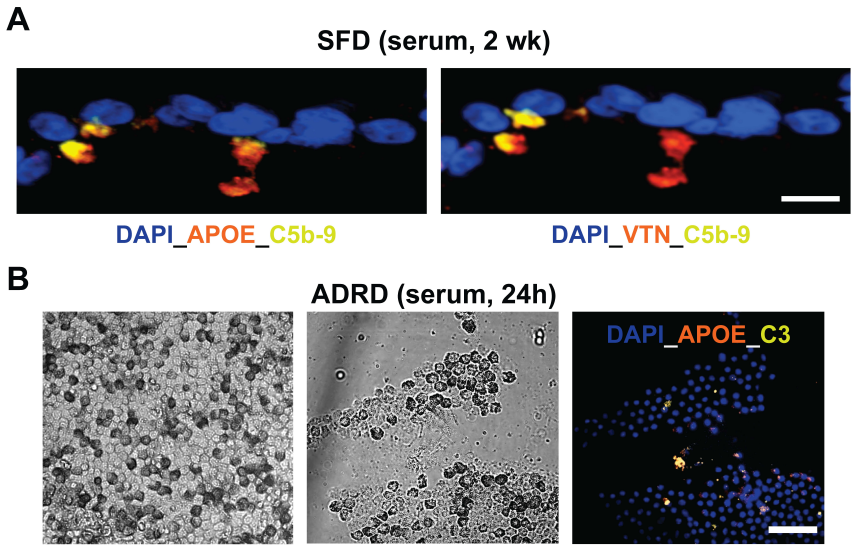

Fig. S9. Serum supplementation affects the composition of sub-RPE deposits underneath "aged" (D90) SFD and ADRD hiPSC-RPE cultures. (A) Immunocytochemical analyses of SFD hiPSC-RPE cross-sections showed co-localization of serum-derived proteins (C5b-9 and VTN) with known drusen marker, APOE, in SFD hiPSC-RPE after chronic serum supplementation (10%, 2 wk) (Scale bar = 25 μm). Of note, the left and right panel display the same SFD hiPSC-RPE section with immunolocalization results for different proteins, APOE and C5b-9 (left panel) vs. VTN and C5b-9 (right panel). (B) Immunolocalization studies also demonstrated co-localization of APOE and complement factor C3 in basal deposits underneath serum-treated (10%, 24h) ADRD hiPSC-RPE cultures. Of note, the left two panels show light microscopy images of ADRD hiPSC-RPE monolayer prior to immunostaining, before (left panel) and after (middle panel) selective removal of a portion of hiPSC-RPE cells in the culture dish. After the removal of ADRD hiPSC-RPE cells (middle panel), the entire dish was immunostained for APOE and C3 (right panel). Furthermore, DAPI staining was used to demarcate hiPSC-RPE cell containing vs. hiPSC-RPE cell void areas on the dish (Scale bar = 25 μm).

A

hiPSC line	Control/ Mutant	Description
Ctrl1	Control	Individual from general population (no macular degeneration)
Ctrl2	Control	Individual from general population (no macular degeneration)
SFD1	Mutant	SFD patient 1
SFD2	Mutant	SFD patient 2
Ctrl3	Control	Unaffected family member of SFD patient 1 and 2
DHRD1	Mutant	DHRD patient 1
DHRD2	Mutant	DHRD patient 2
Ctrl4	Control	Gene corrected hiPSC line for DHRD patient 1
ADRD1	Mutant	ADRD patient 1
ADRD2	Mutant	ADRD patient 2
Ctrl5	Control	Unaffected family member of ADRD patient 1 and 2

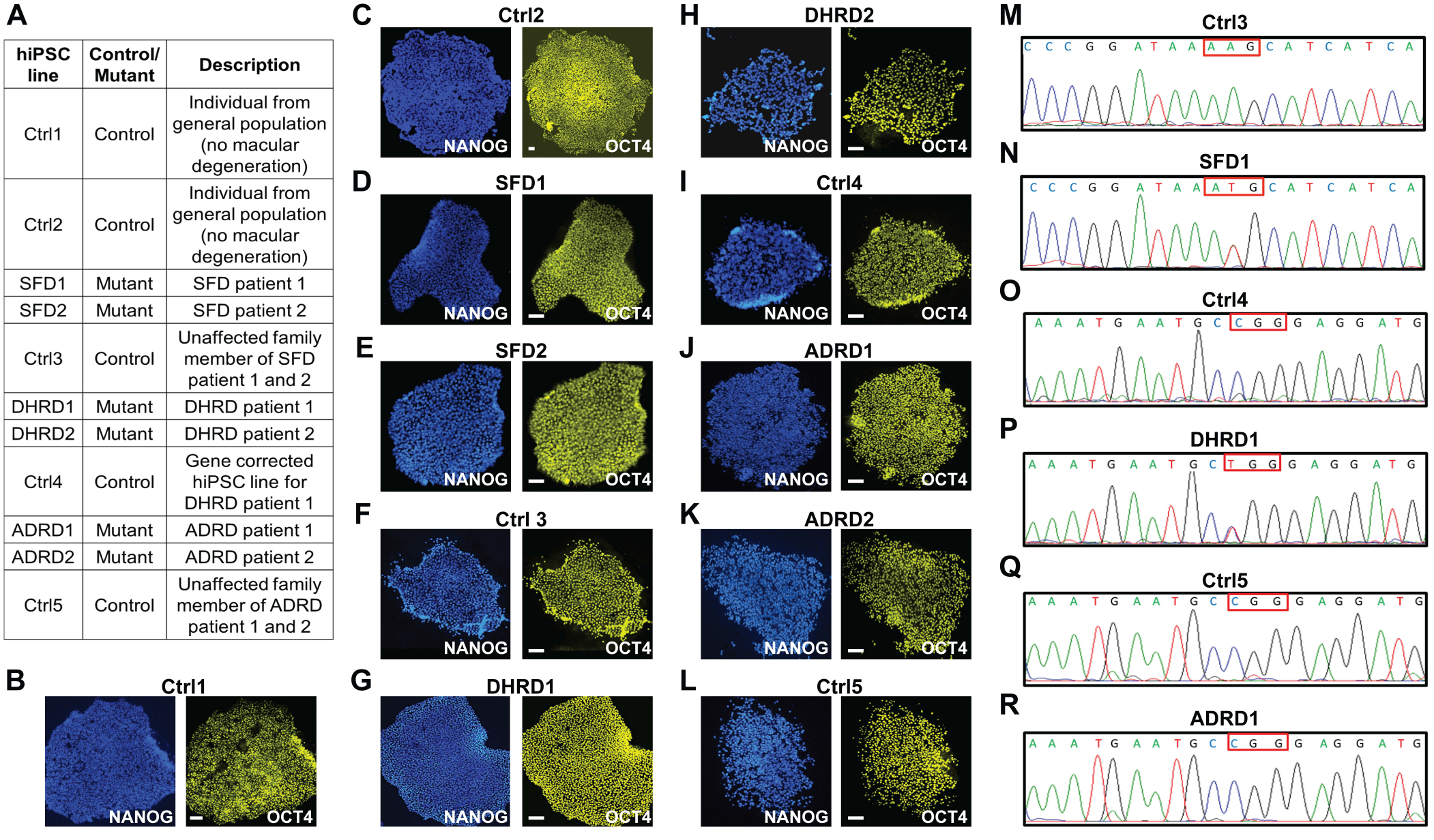

Fig. S10. Characterization of Ctrl and Patient-derived hiPSCs showed robust expression of pluripotency markers in all hiPSC lines and the expected gene mutations in SFD and DHRD hiPSC lines. (A) A table describing all the control and patient-derived hiPSCs utilized in this study. (B-L) Immunocytochemistry analyses demonstrated consistent and robust expression of pluripotency markers, OCT4 and NANOG in all Ctrl and patient-derived hiPSCs. (M-R) Sequencing analyses confirmed the absence and presence of the expected point mutations in the TIMP3 gene (S204C) in Ctrl (M) vs. patient- derived SFD hiPSCs (N), respectively. Similarly, sequencing analysis of confirmed the absence and presence of the expected point mutations in the EFEMP1 gene (R345W) in gene-corrected DHRD hiPSC line (O) vs. corresponding uncorrected DHRD hiPSC-line (P). Sequencing analyses also confirmed the absence of mutation in EFEMP1 gene in hiPSCs derived from ADRD patient and the corresponding unaffected sibling (Q and R) (Scale bar = 100 μm).

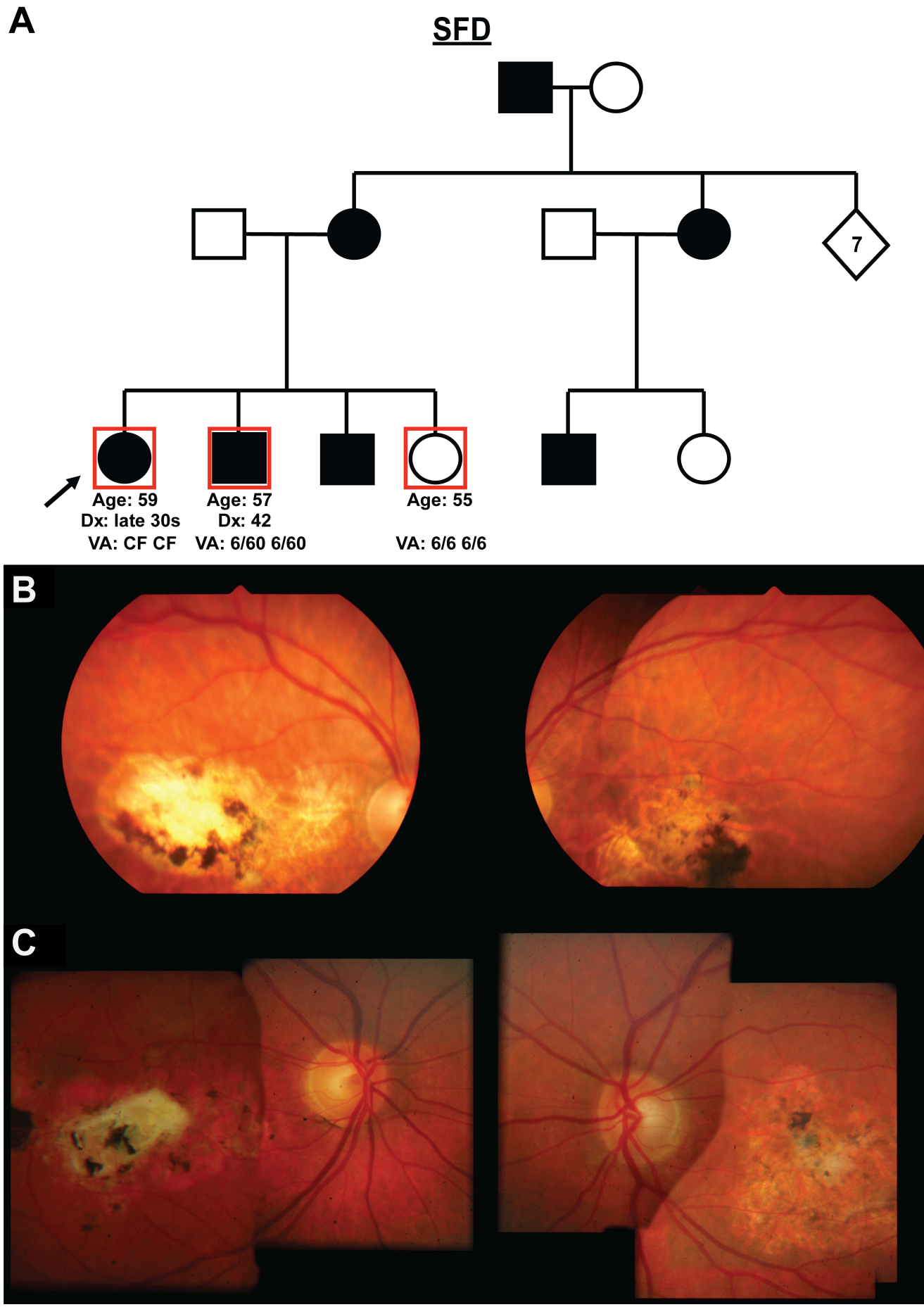

Fig. S11. Pedigree and clinical description of SFD patients. (A) Pedigree chart showing the family structure, patient's age (Age), age at diagnosis (Dx) and best correct visual acuity (VA) at most recent follow-up for SFD patients. Patients utilized in this study are highlighted with a red box and the proband is indicated with a black arrow. (B, C) Representative fundus photographs from the proband (B) and their other affected relative (C) who were included in this study.

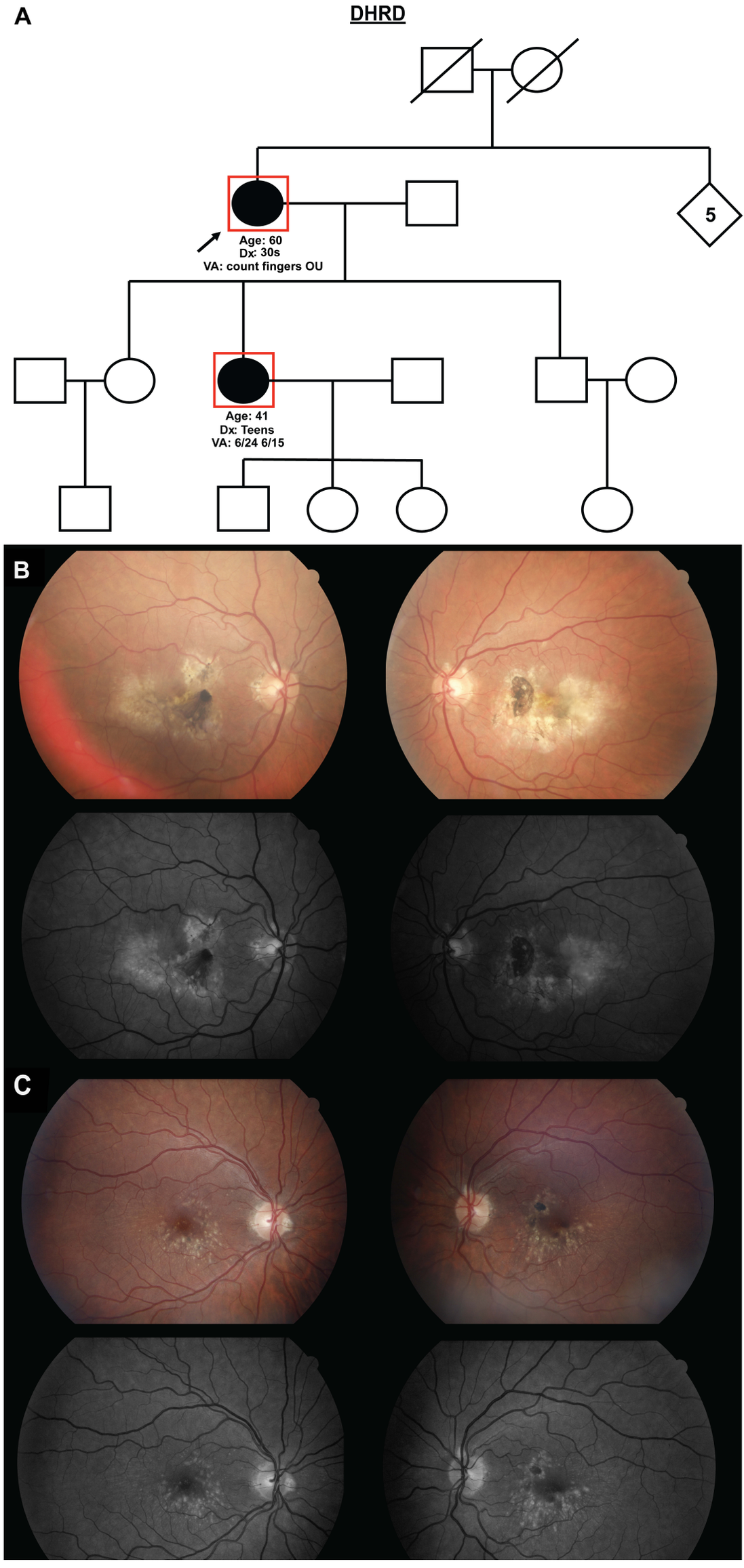

Fig. S12. Pedigree and clinical description of DHRD patients. (A) Pedigree chart showing the family structure, patient's age (Age), age at diagnosis (Dx) and best correct visual acuity (VA) at most recent follow-up for DHRD patients. Patients utilized in this study are highlighted with a red box and the proband is indicated with a black arrow. (B, C) Representative fundus photographs and autofluoresence images from the proband (B) and their other affected relative (C) those were included in this study.

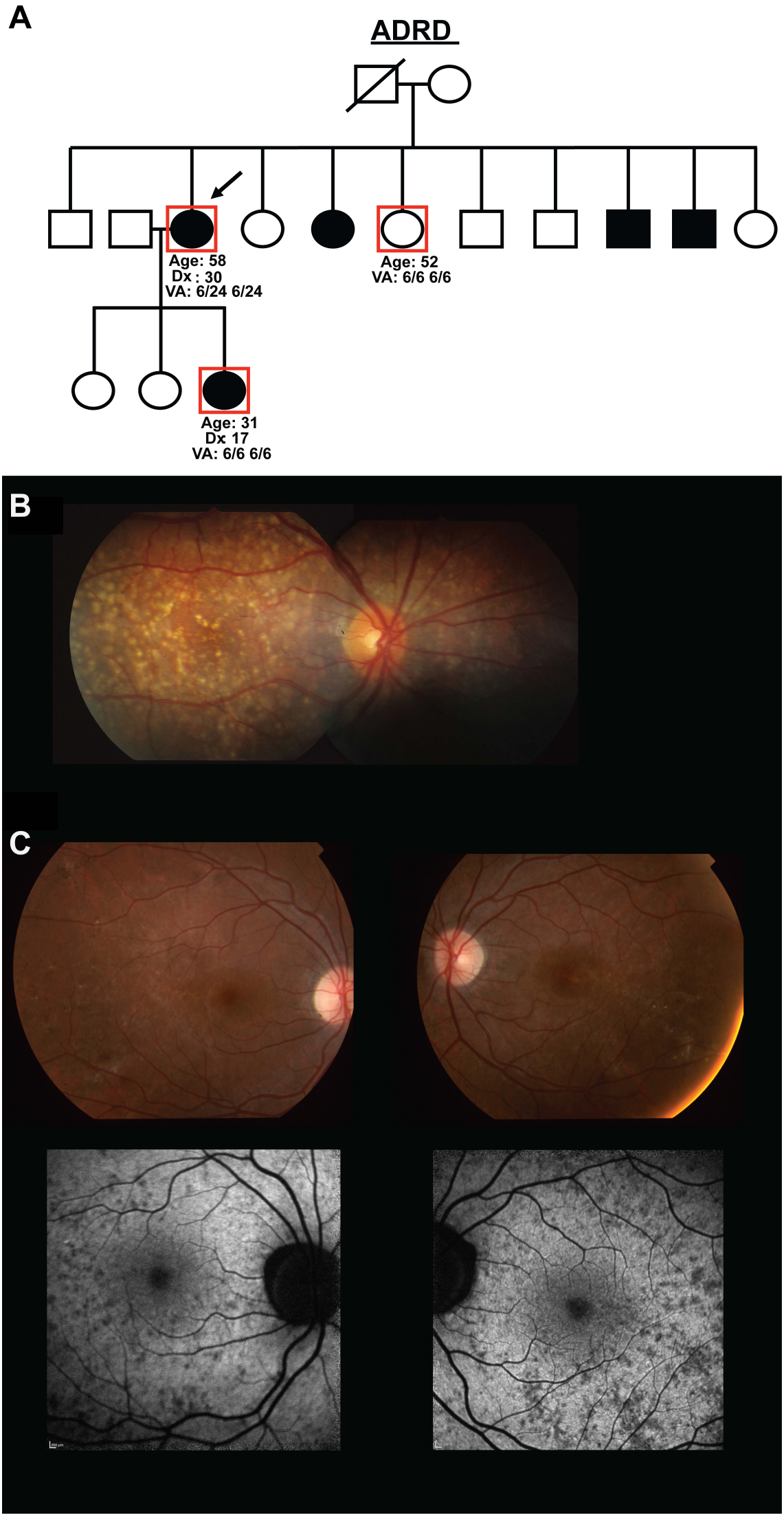

Fig. S13. Pedigree and clinical description of ADRD patients. (A) Pedigree chart showing the family structure, patient's age (Age), age at diagnosis (Dx) and best correct visual acuity (VA) at most recent follow-up for ADRD patients. Patients utilized in this study are highlighted with a red box and the proband is indicated with a black arrow. (B, C) Representative fundus photographs and autofluoresence images from the proband (B) and their other affected relative (C) those were included in this study.

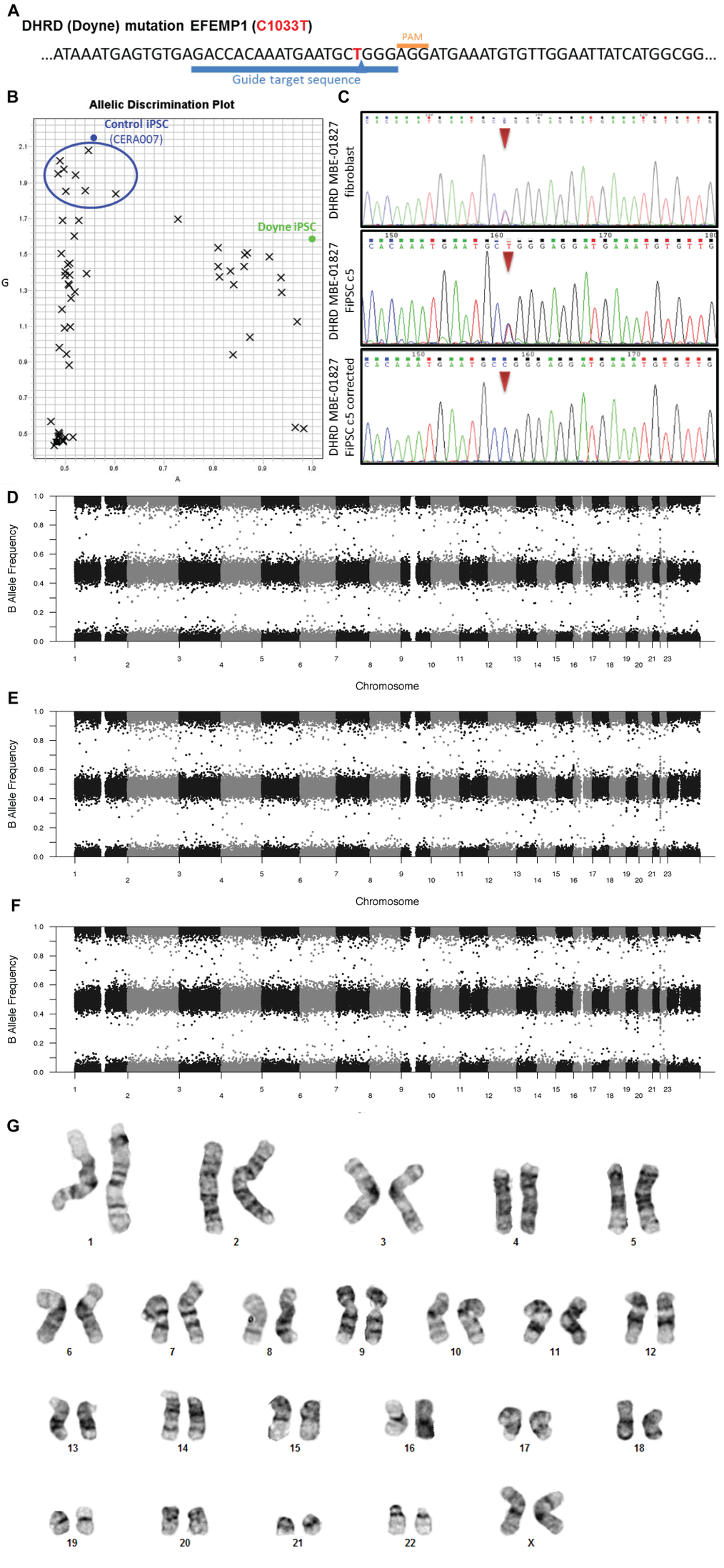

Fig. S14. CRISPR correction and characterization of gene-corrected DHRD patient hiPSCs. (A) Guide RNA target sequence designed over the EFEMP1Arg345Trp (rs121434491; NM_001039348.2:c.1033C>T) mutation site using the CRISPR design tool (http://crispr.mit.edu/). (B) Allelic discrimination plot demonstrated the presence of the corrected cytosine allele in gene-corrected iPSCs versus the mutant thymine allele in the DHRD-patient iPSC. (C) Sanger sequencing confirmed the correction of EFEMP1 mutation in the gene-corrected DHRD hiPSC line. (D-F) Virtual karyotyping confirmed the origin of the gene-corrected hiPSCs from DHRD-patient hiPSCs and no gross gene re-arrangement or chromosomal aberrations were observed in DHRD patient fibroblast (D), DHRD patient hiPSCs (E) and the corresponding gene-corrected hiPSCs (F). (G) Standard karyotyping analysis verified the chromosomal integrity of the gene-corrected hiPSC line.